SPi	Journal Code				Article ID					Dispatch: 26.02.13	CE: Crystal Gayle M. Sarming
	F	F	E		1	2	0	4	8	No. of Pages: 18	ME:

doi: 10.1111/ffe.12048

Q1 Q2 Fatigue crack initiation in Hastelloy X – the role of boundaries

W. ABUZAID[1], A. ORAL[2], H. SEHITOGLU[1], J. LAMBROS[3] and H. J. MAIER[4]

[1]*Department of Mechanical Science and Engineering, University of Illinois at Urbana-Champaign, 1206 W. Green St., Urbana, IL 61801, USA,* [2]*Department of Mechanical Engineering, Yildiz Technical University, 34349 Besiktas, Istanbul, Turkey,* [3]*Department of Aerospace Engineering, University of Illinois at Urbana-Champaign, 104 S. Wright St., Urbana, IL 61801, USA,* [4]*Lehrstuhl für Werkstoffkunde (Materials Science), University of Paderborn, 33095 Paderborn, Germany*

Received in final form 3 October 2012

ABSTRACT In polycrystalline metals, microstructural features such as grain boundaries (GBs) influence fatigue crack initiation. Stress and strain heterogeneities, which arise in the vicinity of GBs, can promote the nucleation of cracks. Because of variations in grain size and GB types, and consequently variations in the local deformation response, scatter in fatigue life is expected. A deeper quantitative understanding of the early stages of fatigue crack nucleation and the scatter in life requires experimental and modelling work at appropriate length scales. In this work, experiments are conducted on Hastelloy X under fatigue conditions, and observations of fatigue damage are reported in conjunction with measurements of local strains using digital image correlation. We use a recent novel fatigue model based on persistent slip band–GB interaction to investigate the scatter in fatigue lives and shed light into the critical types of GBs that nucleate cracks. Experimental tools and methodologies, utilizing *ex situ* digital image correlation and electron backscatter diffraction, for high resolution deformation measurements at the grain level are also discussed in this paper and related to the simulations.

Keywords fatigue crack initiation; grain boundaries; grain cluster; microstructure; persistent slip band.

Q3

NOMENCLATURE

$\mathbf{b_r}$ = the residual Burgers vector due to slip transmission
d = the mean dislocation spacing within the persistent slip band (PSB)
E = Energy of PSB interacting with a grain boundary (GB)
E_{app} = the energy of the stress field due to the applied forces
E_{hard} = the work hardening energy of the material
$E_{interaction}$ = the energy associated with PSB–GB interaction resulting in dislocation pile-ups and steps/ledges at the GB
$E_{lattice\ shearing}$ = the energy for the formation of the PSB by shearing the lattice
$E_{nucleation}$ = the energy to nucleate a dislocation from the GB
$E_{pile-up}$ = the energy of the stress field due to the dislocation pile-ups at the PSB
h = the PSB width
L = the grain size (also assumed to be the length of the PSB)
L' = the grain size of neighbouring grain
L_{cs} = the critical grain cluster size
m = the Schmid factor of the grain containing the PSB
n_{dis}^{pen} = the number of dislocations penetrating the GB
N = the number of cycles
N_{in} = the number of cycles to crack initiation to a critical size
R = fatigue loading ratio
Y = the extrusion height
∂X_i = the slip increment

Correspondence: H. Sehitoglu and W. Abuzaid. E-mail: huseyin@illinois.edu; abuzaid1@illinois.edu

$\Delta\varepsilon$ = applied strain range for fatigue loading
$\Delta\sigma$ = the evolution of the stress range for a constant applied strain range $\Delta\varepsilon$
ε_{xx} = the horizontal strain
ε_{xy} = the shear strain
ε_{yy} = the vertical strain along the loading direction
ρ = the dislocation density within the PSB
σ = the applied stress
Σ = the character of GB in the coincident site lattice notation
$\bar{\tau}$ = internal stress field that dislocations must overcome to deform the material by increment ∂X
τ^{A} = the applied shear stress
τ^{dis} = the stress field created by dislocation dipoles within the PSB
τ^{b} = the hardening within the PSB due to dislocation interaction

INTRODUCTION

Heterogeneous plastic flow and strain accumulation at the microstructural level are precursors to fatigue crack initiation.[1–4] In the absence of material defects such as pores or inclusions, the microstructure of the material, that is, grain size, grain orientation and grain boundary (GB) character, plays an important role in introducing deformation heterogeneities in the material response.[5] Variability in the material at the microstructural level, and consequently in the local deformation response, has been known to contribute to the excessive scatter in the fatigue lives of polycrystalline metals. Several microstructure-based models have been proposed to explain and predict this experimentally observed scatter in life.[6–10] In general, these types of models are based on describing the local, inhomogeneous material response under cyclic loading and proposing a critical condition for crack initiation. Different crack initiation criteria have been introduced that reflect the state of knowledge on the mechanism of crack nucleation and the state variables that can be described either through modelling or experiments. Although significant progress in the modelling aspect has been made, supportive quantitative, full field and multiscale experimental work is limited. These kinds of measurements, for example, the full field experimental measurement of strain evolution at the grain level in fatigue, are challenging but can provide crucial and specific information that will help advance our current knowledge of the early stages of fatigue crack initiation and thus help improve crack initiation models. In the present paper, we aim to explore the scatter in fatigue life for a nickel-based superalloy, Hastelloy X, through experiments and simulations. We also use digital image correlation (DIC) in conjunction with electron backscatter diffraction (EBSD) to make high resolution strain measurements at the microstructural level and evaluate the role of GBs in introducing strain heterogeneities. The experimental observations are discussed in relation to the crack initiation fatigue model used in this work.

Various features (e.g. material flaws, stress concentrations and GBs) and different driving forces can induce fatigue crack initiation.[11,12] In the current work, we are concerned with fatigue cracks initiating in the vicinity of GBs, which as will be seen, is the dominant crack initiation mechanism for the nickel-based superalloy Hastelloy X. It is well known that certain types of GBs are susceptible to crack initiation. Particularly, twin boundaries (TBs), also referred to as Σ3 GBs using the coincident site lattice (CSL) notation, have been identified as preferred sites for fatigue crack initiation.[13–16] Different proposals describing a stress concentration near TBs have been put forward. The stress concentrations arising from slip bands impinging on the TB,[17] TB ledges[15] and the elastic incompatibility across the TB[13,18] have all been used to evaluate the stress field near TBs and explain their tendency to nucleate fatigue cracks.

Several approaches have been proposed to develop models capable of predicting fatigue crack initiation. Some of these models utilize finite element crystal plasticity simulations to describe the local stress and strain fields at the crystal level.[7,9,19–23] The simulation results along with experimental life data were used to predict crack initiation based on the critical accumulated slip[9,23] or based on energy considerations.[22] Other modelling approaches rely on dislocation–GB interaction. The foundation for these types of models goes back to the early work of Lin and Ito,[24] Tanaka and Mura,[25] and Mughrabi and coworkers[26] on persistent slip band (PSB) mechanisms. More recently, significant advances have been made in this field with the use of improved computational tools such as atomistic simulations.

Sangid *et al.*,[27,28] proposed a model for fatigue crack initiation based on the energy of PSB interacting with a GB. The model considers the specifics of the GB structure[29] and the differences in energy barriers for slip nucleation and slip transmission across different GBs[30] and different grain clusters.[28] [Note that the concept of grain clusters, that is, groups of grains connected by low angle GBs (LAGBs), which allow for slip transmission, controlling fatigue damage has been previously addressed in various experimental and numerical studies[5,19,31]]. The ability to determine the critical GB types for fatigue crack initiation as well as the scatter in life is the main strengths of this model.[27,28] In the current work, we will apply this Q5 novel fatigue model, briefly discussed in the Fatigue Model section, to investigate fatigue life scatter in Hastelloy X. We also discuss the critical grain cluster size, both observed and calculated, in Hastelloy X and how it influences the predicted life for crack initiation.

The majority of available experimental work on fatigue investigates the nominal sample response, that is, the average stress–strain or hysteresis loops, life data and postmortem microstructural analysis to determine the possible deformation mechanisms and/or critical microstructural features, for example, GBs, which initiated cracks under cyclic loading.[12,32] Because substantial advances have been made on the modelling side towards microstructural, or even atomistic informed, fatigue crack initiation models,[7] there is a need for high resolution and local deformation measurements to help validate and refine these types of models. The optical technique of DIC provides the means to make such measurements.[33,34] Its extension to high resolutions, as we do in this work, can provide further quantitative understanding of the localized deformation response. Combined with crystal orientation and GB characterization using EBSD,[35] significant insight into the strain localization regions and specific GBs response, for example, shielding or transmitting, and how they influence fatigue crack initiation can be ascertained.[36]

In summary, we demonstrate how physics-based fatigue modelling and high-resolution DIC measurements can be utilized to better understand the role of GBs in fatigue crack initiation and help explain and predict the experimentally observed scatter in life under cyclic loading conditions. To do so, we present high resolution DIC/EBSD results for strain accumulation at the microstructural level and describe how these results can be used to shed light into the specific GB response in blocking or transmitting slip (which leads to the formation of grain clusters). The experimental observations along with scanning electron microscope (SEM) analysis of fatigue cracks in Hastelloy X are used to justify modelling crack Q6 initiation based on PSB–GB interaction (Microstructural analysis of fatigued samples section). Also, life predictions from simulations are obtained using the fatigue crack initiation model and compared with experimental life data for the Hastelloy X subjected to fatigue loading.

MATERIAL AND METHODS

Material and sample preparation

Polycrystalline Hastelloy X was investigated in this study. The alloy was solution heat treated at 1177 °C. Dog bone specimens were electro-discharge machined from a 3.2 mm thick sheet as in the received condition. The sample gauge area was 4.0 × 3.2 mm, and the thickness was 1.5 mm. The surface of each specimen was mechanically polished using SiC paper (up to P1200) followed by finer polishing using alumina polishing powder (down to 0.3 μm) and vibro-polishing with colloidal silica (0.05 μm). The final surface finish was adequate for microstructural surface characterization using EBSD. For microstructure measurements, an SEM equipped with an EBSD detector was used with a measurement spacing of 1 μm. Figure 1a shows a grain orientation map of one of F1 the samples investigated in this study. The total number of grains in the region of interest was 2789 grains with an average grain diameter of ~24. The percentage of annealing TBs (Σ3 type GBs using the CSL notation) was about 30% of the total number of GBs, which corresponds to about 65% of the total CSL content as shown in Fig. 1b.

High resolution digital image correlation measurements

Digital image correlation is an optical technique that uses the comparison between a reference (undeformed) and a deformed digital image of the random speckle pattern on a material surface to measure in-plane surface displacement and strain components.[37] The DIC measurement resolution is highly dependent on the optical magnification at which the reference and deformed images are captured.[34] With increased magnification, accurate strain measurements with sub-grain level resolution can be achieved. The challenge associated with higher magnification imaging is that it reduces the field of view and thus imposes limitations on the area/number of grains that can be studied. The *ex situ* technique used in this study, and described in detail in Ref. [33], addressed this problem and enabled high resolution measurements over relatively large areas by capturing and stitching enough high magnification images to cover the required region of interest.

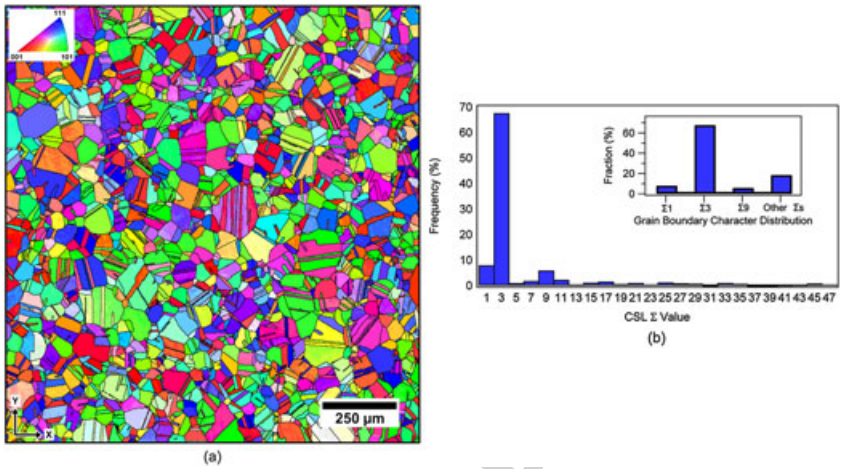

Fig. 1 (a) Grain orientation map from electron backscatter diffraction. (b) Grain boundary character distribution in coincident site lattice (CSL) notation showing a high percentage of annealing twin boundaries (i.e. Σ3 boundaries).

The DIC results reported in this paper were obtained using images captured at either 10× (0.436 µm/pixel) or 25× (0.174 µm/pixel) optical magnifications. In both cases, a fine speckle pattern was achieved by roughening the highly polished surfaces, initially required for EBSD, with silicon carbide powder (1000 Grit). This method for creating the speckle pattern allowed for a subset size of ~9.2 µm and ~4.7 µm for the 10× and 25× magnifications, respectively. The speckle pattern quality, selected magnification and the achieved DIC resolution allows for sub-grain level deformation measurements (average number of DIC correlation points per grain is equal to 600) and enables quantitative analysis of the plastic strain fields in relation to the underlying microstructure of the polycrystalline specimen.

Fatigue testing

Using a servohydraulic load frame, specimens were fatigue loaded to failure in strain control at a rate of 0.4 Hz and a loading ratio, R, of zero. Two strain ranges were tested, 0.8% (four samples) and 1% (four samples). These experimental results were collected to establish the scatter in fatigue life for later comparison with life from simulations obtained using the fatigue model. For samples where DIC measurements were to be performed, we adopted a different loading condition. These samples were loaded in load control, instead of strain control, at a rate of 0.4 Hz, loading ratio, R, of −1 and stress range of 750 MPa. This was chosen to avoid using an extensometer and guarantee that the surface of the sample, where DIC measurements were made, remained exposed and unchanged by any contact from the extensometer. The purpose of these samples was to investigate the local material response and the role of GBs rather than to establish fatigue life for model comparison. Thus, all fatigue life data shown in this work are only from strain control experiments.

Fatigue model

The fatigue model described briefly in this section, and in detail in Ref. [6,27,28], predicts fatigue crack initiation based on PSB–GB interaction. In the formulation of the model, the energy of a PSB interacting with a GB is described, and its stability is used as a criterion for fatigue crack initiation. The energy expression of a PSB evolves with the number of loading cycles and includes both continuum and atomistic terms as shown in the following expression:

$$\begin{aligned} E = & -E_{app}(\sigma, m, L, N) - E_{hard}(\rho, L, N) \\ & + E_{pile-up}(h, d, L, N) + E_{nucleation}(m, \Sigma, h, L, L', N) \\ & + E_{interaction}(m, \Sigma, h, L, L', N) + E_{lattice\,shearing}(L, N), \end{aligned} \tag{1}$$

where σ is the applied stress, m is the Schmid factor of the grain containing the PSB, L is the grain size (also assumed to be the length of the PSB), N is the number of cycles, ρ is the dislocation density within the PSB, h is the width of the PSB, d is the mean dislocation spacing within the PSB, Σ is the character of GB in the CSL notation and L' is the grain size of neighbouring grain. The first three terms in Eq. (1) are based on continuum mechanics concepts for modelling dislocations. These terms represent the energy of the stress field due to the applied forces (E_{app}), the work hardening energy of the material (E_{hard}) and the energy of the stress field due to

the dislocation pile-ups at the PSB ($E_{pile-up}$). The PSB structure consists of a number of dislocation layers (i.e. planes at which dislocations glide), and each plane within the PSB has individual contribution to the continuum terms. Energy from these terms represents an internal barrier that should be overcome by dislocations in order to deform the material plastically. The remainder of the terms in Eq. (1) are computed from atomistic simulations and represent the energy to nucleate a dislocation from the GB ($E_{nucleation}$), the energy associated with PSB–GB interaction resulting in dislocation pile-ups and steps/ledges at the GB ($E_{interaction}$) and the energy for the formation of the PSB by shearing the lattice ($E_{lattice\ shearing}$). GBs act as sources of dislocations that are agglomerated in the PSB, and they act as barriers for slip transmission. Each GB has a different energy barrier for dislocation nucleation and dislocation penetration depending on its character. These atomistic energies are incorporated into the evaluation of $E_{nucleation}$ and $E_{interaction}$. The dislocation must overcome an energy that can be associated with destroying the lattice stacking sequence in the matrix to form slip bands by cutting the matrix. This energy corresponds to the stacking fault energy that is incorporated into the evaluation of $E_{lattice\ shearing}$. Writing the energy expression as shown in Eq. (1) allows us to consider the main microstructural features that influence fatigue crack initiation. For example, the Schmid factor, which is related to crystal orientation and loading direction, and grain size are included in the continuum terms of Eq. (1). By incorporating the atomistic terms, the differences in response between the various types of GBs (different CSL) are also accounted for. This is important if we want to accurately capture and explain some of the previous experimental results on certain types of GBs, particularly Σ3 TBs, which have been reported as preferred sites for fatigue crack initiation.[13–15,38]

The criterion for when fatigue crack initiation occurs is based on the stability of the PSB. Each of the energy expressions in Eq. (1) can be expressed in terms of the slip increment (∂X_i), which is defined schematically in the inset drawing of Fig. 2. To check for the stability of the PSB, the derivatives of the PSB energy terms with respect to the slip increment are computed. As loading progresses, the calculated derivatives will evolve with the number of loading cycles as illustrated in Fig. 2 for one of the Hastelloy X simulations conducted in this study. The coloured lines represent the evolution of each of the individual energy terms in Eq. (1), and the black line corresponds to the total energy that is calculated by adding the contributions from all of the individual components (i.e. from the coloured lines). Eventually, initiation is predicted once the magnitude of the total energy derivative reaches zero in addition to the second derivative being positive in order to insure that the energy corresponds to a local and stable minimum, expressed by

$$\frac{\partial E}{\partial X_i} = 0. \tag{2}$$

The methodology described earlier for predicting crack initiation based on PSB–GB interaction is also

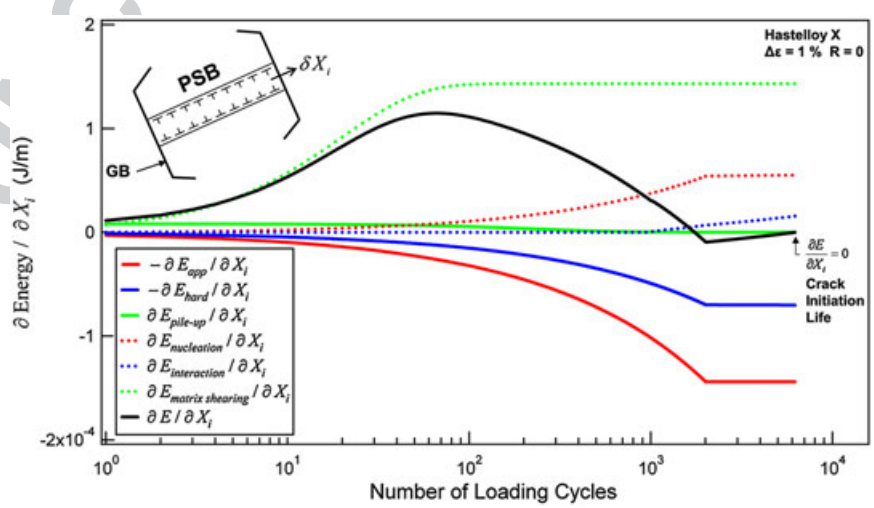

Fig. 2 The evolution of the individual (coloured lines) and total (black line) energy rate terms shown in Eq. (1) with increasing loading cycles. Each term is expressed as the energy derivative with respect to the slip increment, ∂X_i (∂X_i shown in the inset figure). Initiation is predicted once the total energy reaches a stable minimum (i.e. its derivative is zero) in addition to the second derivative being positive (marked with an arrow in the figure).

applicable to polycrystals. In this case, the energy equation is evaluated for each grain in the aggregate or for each grain cluster, that is, group of grains connected with LAGBs. LAGBs allow PSBs to traverse the GB (i.e. slip transmission), thus increasing the length of the PSB and consequently influencing the energy terms in Eq. (1). On the basis of this condition for slip transmission (i.e. slip passing through a LAGB), EBSD measurements of grain orientations can be easily used to construct the grain clusters as detailed in Appendix D in Ref. [28]. It should be pointed out, however, that other types of GBs (e.g. Σ3 GBs) can, under certain conditions (e.g. high resolved shear stress and low residual dislocation as discussed in Ref. [40]), allow slip to penetrate through the interface and potentially result in the creation of a grain cluster. In our application of the model, we do not account for this, and the grain clusters are strictly defined using the concept of LAGBs. Once the grain clusters are defined on the basis of EBSD measurements, the number of cycles to crack initiation for each grain or grain cluster is evaluated in the model, and the minimum calculated number of cycles is considered as a limiting case that determines the life of the aggregate.

The calculated life for a polycrystalline aggregate pertains to that particular microstructure, that is, the spatial distribution of grain size, orientation and GB character that is established from EBSD. By spatially varying the microstructure through simulations and reevaluating the life for each of the simulated microstructures, the scatter in fatigue life can be predicted (here, we strictly refer to the scatter introduced by the microstructure). In our application of this model, each of the simulated microstructures is derived from the same experimental EBSD measurements of Hastelloy X, but with the grains spatially rearranged. Using the EBSD data (~2700 grains in this study), the distribution of grain size, Schmid factor (which relates to grain orientations), number of neighbouring grains (each grain is surrounded by a different number of grains) and the GB character (CSL Σ value) are established. These distributions are used to help generate simulated microstructures that are statistically equivalent to the EBSD measurements. Each simulated microstructure consists of a certain number of grains (i.e. a subset of the EBSD data, 350 grains in this study). For each grain, the grain size, Schmid factor and number of neighbouring grains are assigned, and the information of the neighbouring grains is selected from the measured distributions until the required number of grains is reached in the simulated aggregate (350 grains). This process of creating a simulated microstructure is repeated to generate a large number of aggregates (300 in this study) that we evaluate the life for each.

RESULTS

Microstructural analysis of fatigued samples

In this section, we provide some microstructural SEM and transmission electron microscope (TEM) analysis of fatigued Hastelloy X samples. The aim is to investigate the deformation and crack initiation mechanisms and provide justification for using the PSB–GB initiation model described previously for the alloy under consideration here. SEM analysis of samples loaded in fatigue, but interrupted prior to sample failure, reveal that micro cracks predominantly initiate in the vicinity of slip band–GB interaction regions as shown for example in Fig. 3a. We also note that the material exhibits planar slip as shown by the TEM image in Fig. 3b. The observations F3

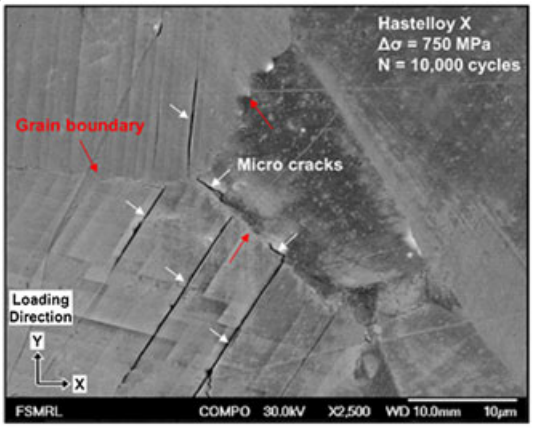

(a)

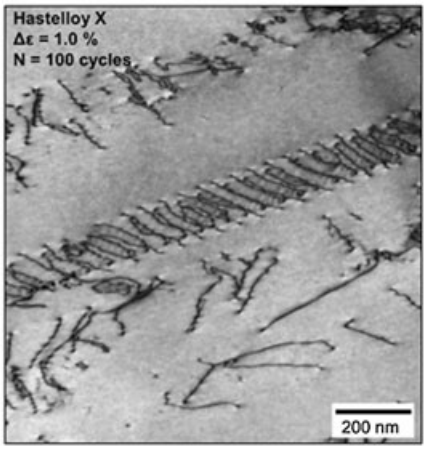

(b)

Fig. 3 (a) Scanning electron microscope micrograph showing micro cracks in the vicinity of slip band–grain boundary interaction regions resulting from fatigue loading prior to sample complete failure. (b) Transmission electron microscope image showing *planar slip* for Hastelloy X.

Colour online, B&W in print

we make on fatigue cracks in Hastelloy X supports our approach to model fatigue crack initiation using the model described in the Fatigue Model section. In the next section, we provide further insight into the applicability of the model, primarily on the deformation by grain clusters, using DIC.

High resolution strain measurements

Q7 Following the *ex situ* DIC procedure described briefly in the High Resolution Digital Image Correlation Measurements section and in detail in Ref. [33], high resolution strain measurements were made on Hastelloy X samples loaded either in uniaxial monotonic tension or in the stress
F4 controlled fatigue loading described earlier. Figure 4a shows a contour plot of the vertical strain field ε_{yy} from a monotonic uniaxial tension test. This component of the strain tensor along with two other components, the horizontal strain field ε_{xx} and the shear strain field ε_{xy}, were measured using DIC. Because we make these strain measurements *ex situ*, with the sample being unloaded, the measured strain components are considered residual plastic strains (note that although elastic strains may exist, their magnitudes are likely to be small). Crystallographic orientation from EBSD was numerically overlaid on the DIC strain data utilizing the fiducial markers that permit accurate alignment. As a result, for each DIC measurement point, the crystal orientation is determined from EBSD. This also allows us to accurately overlay the GBs on all the strain contour plots.

The full field strain results show a high level of heterogeneity in plastic strain accumulation, although the loading is uniaxial tension. Differences in strain magnitudes are observed even within single grains with regions in the vicinity of GBs, that is, GB mantles, and regions away from GB, that is, cores, exhibiting variations in the measured strains. Focusing on the GB mantles, the regions close to GBs, we observe that both the highest and the lowest measured strains are found in the GB mantles. On the basis of this observation, we can classify each boundary as a transmitting boundary, if high strains are measured in both mantles across the interface (high–high mantle strains), or a blocking boundary if high strains are measured on only one side of the GB (high–low mantle strains). Examples of these two cases (the regions marked as 'Transmission' and 'Blockage' in Fig. 4a) are shown in Fig. 4b and c, respectively. We note that in both cases, the GBs are Σ3 GBs. Nevertheless, and despite the similarity in GB character, a different response is observed from DIC local measurements. Relating these two

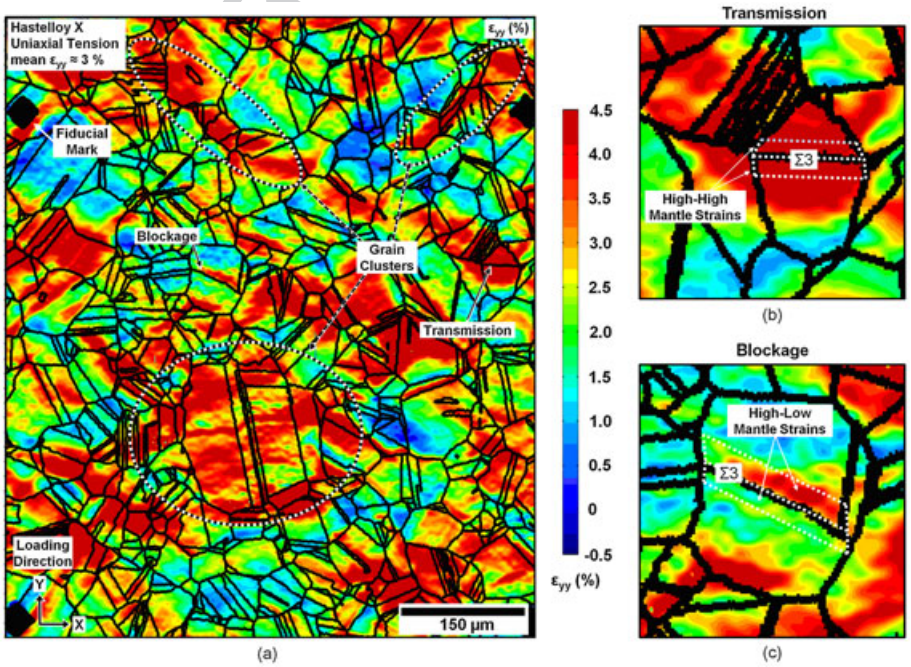

Fig. 4 (a) High resolution strain field, ε_{yy}, along the loading direction, for a sample loaded in uniaxial tension. Grain boundaries (GBs) from electron backscatter diffraction are overlaid on the strain contour plot. Some regions show high strains localizing and extending through multiple GBs, denoting the formation of grain clusters (examples are highlighted in (a)). (b) High strains across a GB can be associated with slip transmission across the GB (which is necessary to form a grain cluster). (c) High strain on one side of the GB can be an indication of blockage or the formation of a pile-up. The GB character for both of the examples shown in (b) and (c) is Σ3, yet the observed response from DIC measurements is different.

examples to the fatigue model used in this study, we note that the blockage case (Fig. 4c) can be a result of slip interacting with a GB and creating a pile-up as considered in the fatigue model. The transmission case (Fig. 4b) indicates slip transmission across the GB and is consistent with the concept of grain clusters in which a PSB can form over multiple grains by transmitting through some GBs. Further evidence of the formation of grain clusters is observed in Fig. 4a; in certain regions, we clearly notice that high strains localize and extend through multiple GBs. These regions are typically isolated and surrounded by low strain regions. Some of these features are marked F5 in Fig. 4a as an example. Figure 5a shows an enlarged view of one of the grain clusters – the lower one – marked in Fig. 4a. The details of slip penetrating the GBs (Σ3 in this case) are clear in this figure. SEM analysis of the same region provides support for this conclusion by showing continuous slip traces across the Σ3 GBs as shown in Fig. 5b. The experimental results presented in Figs 4 and 5 provide clear evidence for the formation of grain clusters and support our modelling approach.

Strain evolution in fatigue

The results presented in the High Resolution Strain Q8 Measurements section for uniaxial tension indicate that GBs play an important role in introducing plastic strain heterogeneities. Observations that indicate slip blockage (pile-up formation) and slip transmission (leading to the formation of grain clusters) were made. In this section, we present some results obtained under cyclic loading conditions to further explore the role of GBs in fatigue. F6 Figures 6a–c show contour plots of the vertical strain field ε_{yy} (along the loading direction) at 1000, 10 000 and 30 000 cycles, respectively, of a fatigue loaded sample, in load control, at a rate of 0.4 Hz, loading ratio, R, of −1 and stress range of 750 MPa. These results were obtained using the same *ex situ* procedure used for the uniaxial tension case but at a lower measurement resolution [10× (0.436 μm/pixel) versus 25× (0.174 μm/pixel)] to allow the investigation of a bigger region of interest, thus giving a higher probability of capturing the region that eventually initiates cracks. For each measurement, the sample was removed from the load frame, and the deformed images were captured in the optical microscope. Subsequently, the sample was reinstalled in the load frame for additional loading.

In addition to similar observations as in uniaxial tension (Figs 4 and 5), the full field contour plots in Fig. 6 clearly show that specific regions accumulate strain with additional loading cycles, whereas other regions remain relatively unchanged with no significant strain evolution. GBs delineate these regions and again indicate the formation of grain clusters and blockage with high strain accumulation on one side of the interface. The role of GBs in strain accumulation is further clarified by monitoring the strain evolution in the vicinity of a specific GB, as shown in Fig. 6d (the GB region selected is shown in the inset of Fig.6d). We measure an increase in strain at that particular boundary while noting that the nominal (average) strain for the entire sample was relatively constant with increasing loading cycles (0.06 and 0.09% at 1000 and 30 000 cycles, respectively). This observation highlights how nominal sample response (e.g. average strain) is inadequate to capture deformation localization and the increased level of

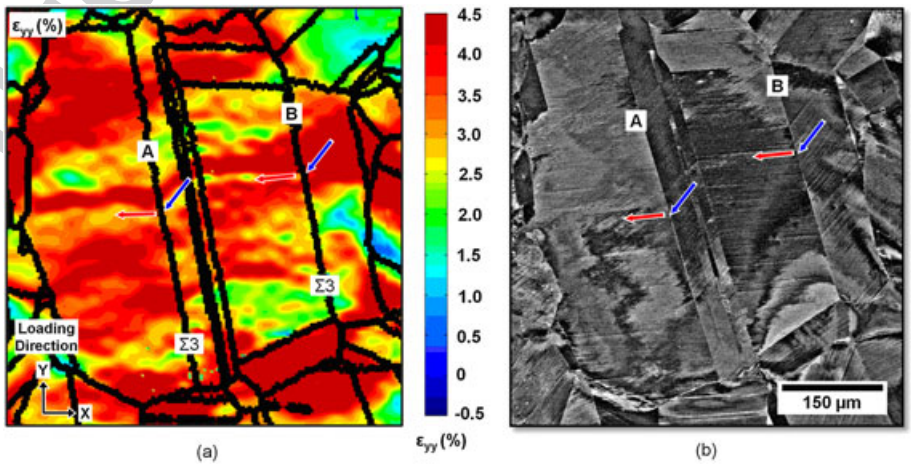

Fig. 5 (a) An enlarged view of the lower of the three grain clusters marked in Fig. 4a. The ε_{yy} strain contour plot shows high strains across multiple Σ3 grain boundaries (GBs). (b) Scanning electron microscope micrograph of the same region in (a) showing continuous slip traces across the same GBs with high measured strains. The results in (a) and (b) provide evidence of slip transmission across the GBs that leads to the formation of a grain cluster.

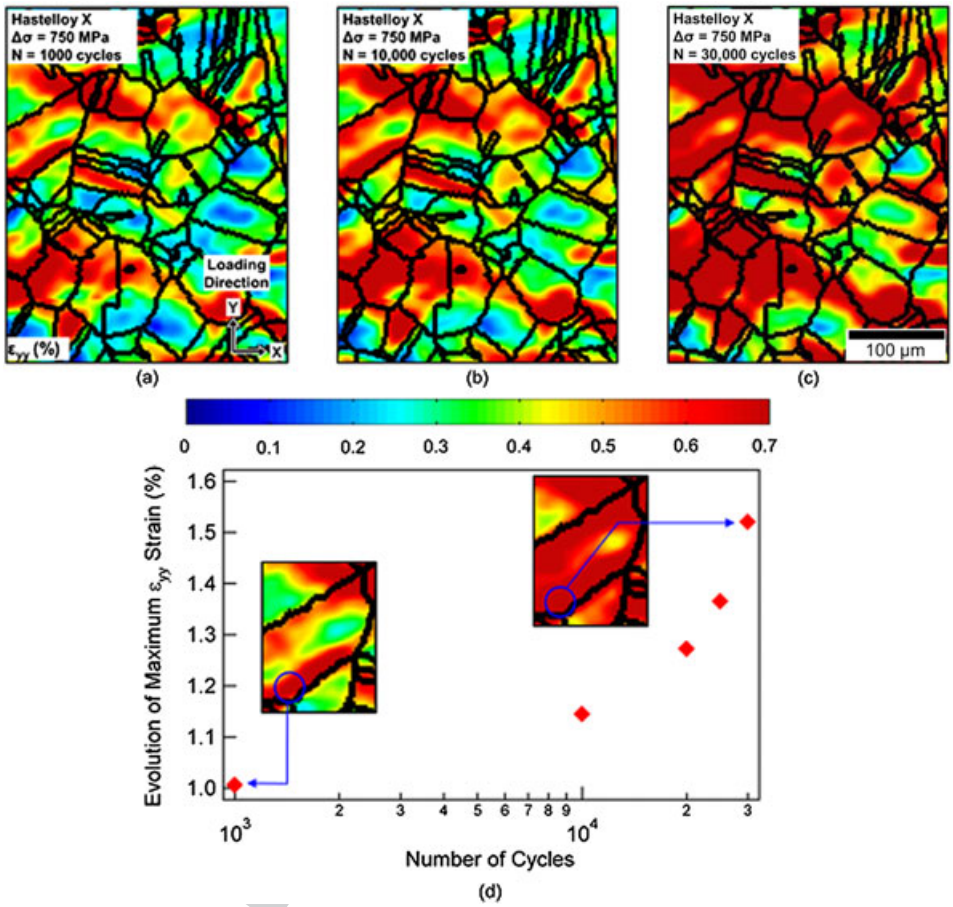

Fig. 6 (a)–(c) Contour plots of the vertical strain field ε_{yy} (along the loading direction) at 1000, 10 000 and 30 000 cycles, respectively. We observe that particular regions, in the vicinity of grain boundaries (GBs), accumulate strain with additional loading cycles, whereas other regions remain, relatively, unchanged with no significant strain evolution. Strain evolution with loading cycles in the vicinity of a single GB is shown in (d). An increase in strain in that particular region is seen, whereas the nominal (average) strain of the entire sample remains relatively constant.

heterogeneity that develops with additional loading. The DIC results provide such quantitative insight during fatigue. The quantitative correlation between such measurements and crack initiation has not been established experimentally in this work and will be perused in a future effort. Nevertheless, the results obtained in fatigue provide additional support for our modelling approach that is based on PSB–GB interaction that leads to fatigue crack initiation at *particular* GBs.

Scatter in fatigue life

F7 Figure 7a shows stress–strain curves for selected cycles of one of the Hastelloy X samples loaded in fatigue ($\Delta\varepsilon = 1\%$, $R = 0$). We observe material hardening in the initial (about 100) cycles, that is, the increase in the stress range seen in Fig. 7a, and more clearly in Fig. 7b, for cycles 1–100, followed by softening until failure. The rate of softening was linear up to the point where a major crack developed in the sample resulting in a sharper and more pronounced stress drop with additional loading cycles. The fatigue lives that we report in this study represent the number of cycles at which this transition was observed, although all samples were fatigue loaded to complete failure (see Fig. 7b for a pictorial illustration of this definition of 'fatigue life'). SEM analysis of the failed samples revealed numerous micro cracks on the sample's surface (across the entire gauge section) in addition to the main crack causing failure (a representative case for one of the tested samples is shown in Fig. 8a). As F8 we indicated earlier (Fig. 3a, notice that no major/main crack has developed in that case), these micro cracks clearly initiate in the vicinity of GBs, that is, along slip bands and around slip band–GB interaction regions. Two different strain ranges were tested in the current work, 0.8 and 1.0%. The fatigue lives for the 0.8% strain

amplitude ranged from 8200 to 14 000 cycles and for the 1.0% strain amplitude between 3200 and 8000 cycles.

Life predictions from simulations

On the basis of the microstructure characterized using EBSD (Fig. 1a), we evaluate the number of cycles to nucleate a crack (GB life) for each grain cluster using the fatigue model described earlier. The term 'GB life' as used in the current paper refers to the number of cycles to nucleate a crack at the PSB–GB interaction region that spans the length of the grain cluster. A selected region of the entire EBSD scan is shown in Fig. 9a. The predicted GB life (N_{GB}) is plotted spatially for this region in Fig. 9b. Different GB colours indicate different life ranges that are defined in the legend of this figure. The GBs coloured with red correspond to lives less than 15 000 cycles, blue GBs represent lives between 15 000 and 50 000 cycles and finally the black boundaries have lives exceeding 50 000. Many of the red marked GBs

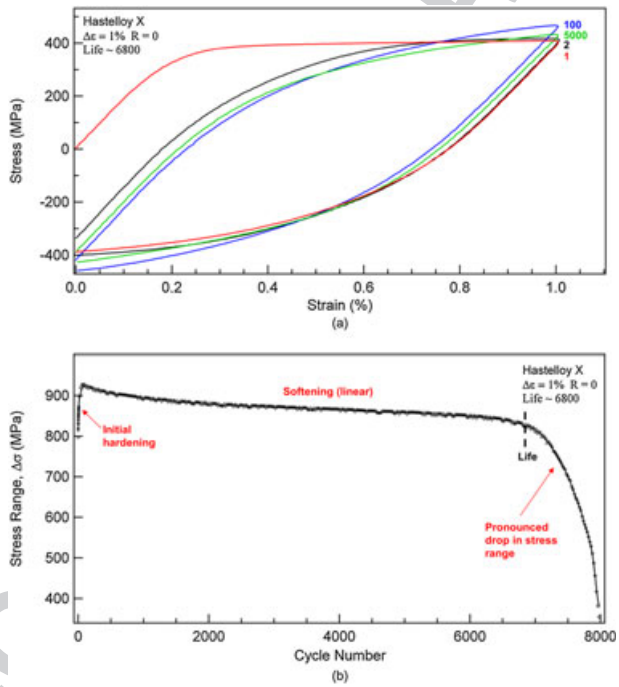

Fig. 7 (a) Stress–strain response for selected cycles. Initial hardening is observed followed by softening. Colours indicated particular cycle numbers. (b) Stress range versus fatigue cycle number (for the same sample as shown in Fig. 7a). Initial hardening is observed followed by a linear softening. Once a major macrocrack has developed, accelerated drop in stress range is seen with additional loading cycles. The life of the sample was assumed to correspond to this transition point as marked in the figure.

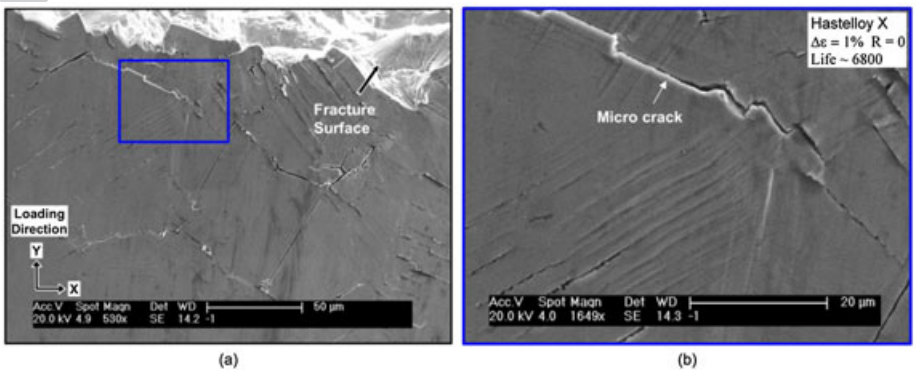

Fig. 8 (a) Scanning electron microscope micrograph of the sample shown in Fig. 7 after failure. Both the sample's surface and the fracture surface are shown. (b) Higher magnification image of the region marked in (a) with a rectangle.

Colour online, B&W in print

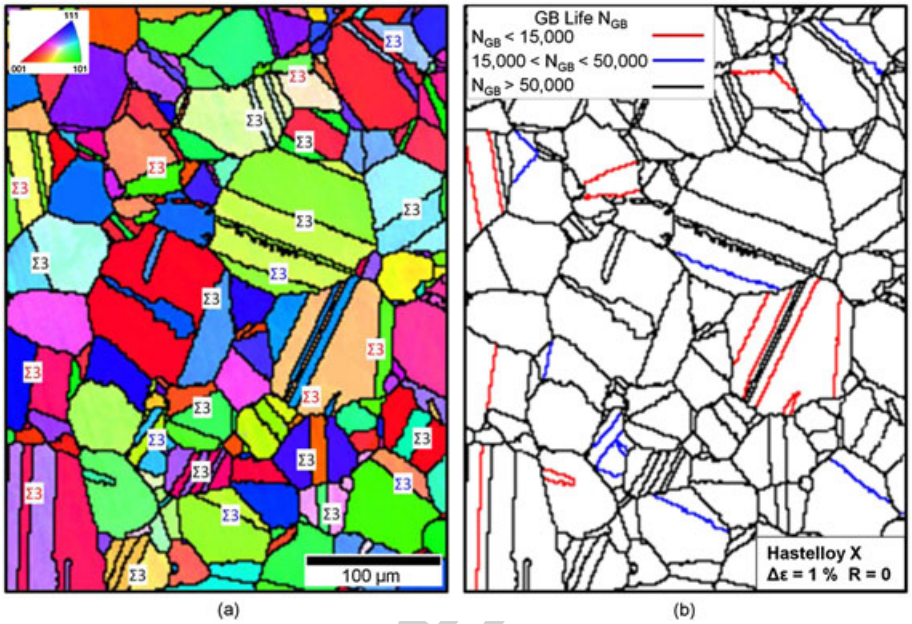

Fig. 9 (a) Grain orientation map of a selected region. This information is utilized by the fatigue model to predict the number of cycles for crack initiation (grain boundary (GB) life) as shown in (b) for 1% applied strain range. Many of the red marked GBs (life <15 000) are Σ3 twin boundaries but a short life is not predicted for all the Σ3 GBs in the simulation.

(life <15 000) are Σ3 TBs, which is consistent with experimental observations of their tendency to nucleate fatigue cracks. We emphasize that short lives are not predicted for all of the Σ3 GBs. Depending on the energy terms described in Eq. (1), each particular Σ3 GB, and each GB in general, will have a different predicted life.

Figure 9b displays the number of cycles to reach a critical state of initiation for each GB. The GB with minimum number of cycles to initiation dictates the life of the aggregate (from the simulation). This life corresponds to a PSB reaching a stable minimum energy configuration and resulting in crack initiation at the PSB–GB intersection region (due to the formation of steps/ledges). The crack length is not defined in the model formulation although one may expect that following initiation at the PSB–GB interaction region, the crack will grow to the PSB length (cluster length) within a relatively short number of cycles (Fig. 3a shows evidence of crack initiation in slip–GB interaction region that extends along the slip trace). In this work, we compare the life from simulations with experimental life Q9 results, which, recall, as defined in the Scatter in Fatigue Life section is not the life to complete failure. Because a crack length is not defined in both cases, some deviation between the lives established experimentally and through simulation is likely. Nevertheless, we expect that the difference between the number of cycles to generate a crack length on the order of the cluster size (multiple grains) to be close to the life as defined in our experiments.

The microstructure characterized using EBSD is then varied to create simulated microstructures (see Fatigue Model section). By reevaluating the life for each of the simulated aggregates, we predict a scatter in fatigue life. The number of cycles for fatigue crack initiation, as predicted from the model (red diamonds), and the experimental life data (black triangles) for different strain ranges are plotted together in Fig. 10a. The simulations F10 are established from 300 different simulated aggregates at three different strain ranges, 1.2, 1.0 and 0.8% applied strains. The experimental results are given for 1.0 and 0.8% applied strain ranges. Experiments at 1.2% were not possible with the sample dimensions used in this study. The 1.2% simulations are included to show the prediction capability of the model outside the range tested. The modelling approach yields good predictions of the experimental scatter in fatigue life (about 85% of the simulated life predictions are within the range of the set of experimental values).

The scatter in life from simulations is introduced by variations in the simulated microstructures (i.e. difference in grain size, GB character, GB neighbour information and Schmid factor). The critical grain clusters that exhibit the minimum life can be in the form of a single grain or a group of grains that are connected with slip transmission permitted at LAGBs. Slip transmission through multiple GBs increases the cluster size and continues until slip is impeded, thus creating a pile-up, by a blocking high angle GB. Therefore, critical

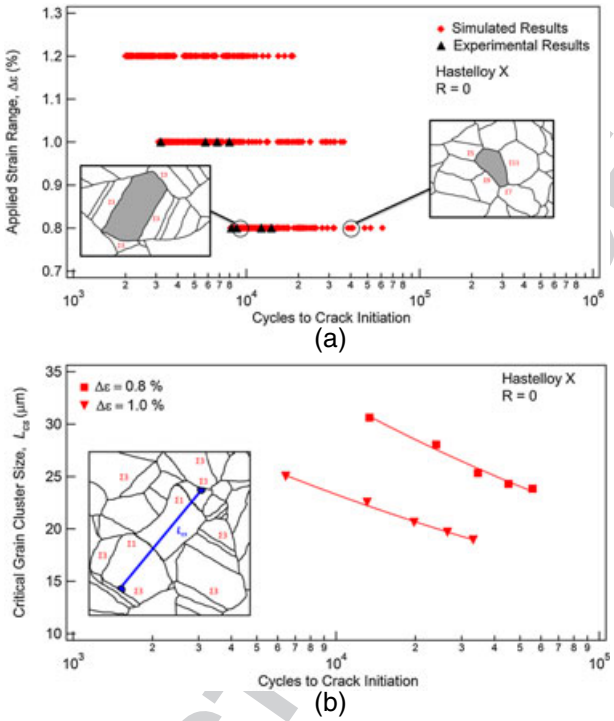

Fig. 10 (a) The number of cycles for fatigue crack initiation, as predicted from the model (red diamonds), and experimental life data (black triangles) for different strain ranges. The simulations are established from 300 different simulated microstructures. The inset to the left shows a grain cluster with a low number of cycles to crack initiation. This grain cluster is comprised of a large grain surrounded by smaller grains, and its grain boundary characteristics are mainly Σ3 twins. The grain cluster shown in the inset to the right has equiaxed grains, with no Σ3 twin boundaries and exhibits a longer predicted life. (b) Critical cluster size versus number of cycles for fatigue crack initiation at different applied strain ranges. The size of the grain cluster where fatigue crack initiation is predicted decreases with increasing cycles to crack initiation.

grain clusters are typically surrounded by high angle GBs (e.g. Σ3) where blockage occurs. The implication of the increase in cluster size as stated earlier is that it increases the length of the PSB and, consequently, the energy terms in Eq. (1). The shaded grain clusters shown in the insets of Fig. 10a show the extreme cases where crack initiation is predicted. The grain cluster on the left with lower cycles to crack initiation corresponds to a large grain surrounded by smaller grains, and its GB characteristics are mainly Σ3 TBs that exhibit the highest energy barrier for slip transmission. The grain cluster on the right with higher cycles to crack initiation is surrounded by almost equiaxed grains and with no Σ3 TBs.

The effect of the critical grain cluster size, L_{cs}, on fatigue crack initiation is illustrated in Fig. 10b. In this figure, the inset schematically shows a representative grain cluster and its size, L_{cs}. This grain cluster consists of three grains that are connected by Σ1 LAGBs. To obtain the data points in Fig. 10b, the entire range of cycles to crack initiation for each strain range in Fig. 10a is divided into five equal intervals (binned based on number of cycles to crack initiation). Then, mean values of critical grain cluster size and mean values for cycles to crack initiation within each interval are plotted in Fig. 10b. The size of the grain cluster where fatigue crack initiation is predicted decreases with increasing number of cycles to crack initiation. The following equation is obtained by fitting to the simulations results in Fig. 10b,

$$\Delta\varepsilon = 0.128\, N_{in}{}^{-0.09}\, L_{cs}{}^{-0.55}, \tag{3}$$

where $\Delta\varepsilon$ is the applied strain range, N_{in} is the number of cycles to crack initiation to a critical size and L_{cs} is the critical grain cluster size in μm. Similar to the Hall–Petch type relation, Eq. (3) exhibits almost a square root dependence for the grain cluster size. The results presented in Fig. 10b, which lead to Eq. (3), represent a statistical approach to examining the importance of the microstructural attributes considered in the fatigue model, in this case the cluster size, on the number of cycles to crack initiation. Similar analysis on the other contributing factors can help us identify the key parameters that have the largest influence on the calculated life.

DISCUSSION

Consideration of the microstructural features that induce local inhomogeneity in the material response, and thus create conditions that facilitate the nucleation of fatigue cracks, is vital for the development and refinement of crack initiation models. In the current work, we utilize EBSD to describe the microstructure of polycrystalline Hastelloy X, that is, GB types and grain sizes, and use that information in a fatigue crack initiation model. We also use EBSD data to enable high resolution experimental measurements in relation to the microstructure. In the model, the energy of PSBs interacting with GBs was considered, and in the experiments, the strain in GB regions and the formation of grain clusters were observed. We believe that analysis at the scales considered here, experimentally and through simulation, can give us new insights into the early stages of fatigue crack initiation and help refine model predictions. For example, by consideration of EBSD, the model selects the most favourable conditions for crack nucleation from a cluster of grains. Verification of model predictions from experiments (locally, for the particular regions where initiation is predicted) is possible through strain measurements at the mesoscale (using *ex situ* DIC) and will be pursued in future efforts.

The model prediction for the scatter in life is in good agreement with the experimental results plotted in Fig. 10a. Despite the fact that simulation results show a higher limit for life compared with that captured by the experiments, about 85% of the simulated results are within the range of the experimental values. A possible cause for the deviation may be from the fact that the life as established from experiments does not correspond exactly to the crack initiation life. A crack growth portion must be present and is not accounted for in the procedure for determining the life as shown in Fig. 7b. The contribution to life from crack growth, compared with initiation, is obviously dependent on the loading conditions (i.e. more important in high cycle fatigue compared with low cycle fatigue). Nevertheless, being able to remove (subtract) the crack growth portion from the established life will enable a more reliable comparison with model predictions and will also help evaluate the accuracy of the current approach for determining life experimentally. High resolution *in situ* experiments, or interrupted *ex situ* experiments, will be required to address this issue. Such an effort will be pursued in future work where we will also monitor strain evolution locally prior to crack initiation. Other factors can also contribute to the observed deviation between experimental and simulation results, for example, the model does not capture the local stress state (i.e. we are not solving the initial boundary value problems for local/grain level stress state). Further analysis will be required to evaluate and address this issue.

The predicted GB life plots shown in Fig. 9b can be useful in the visualization of the critical location for crack initiation. It is observed that Σ3 TBs are the favourable fatigue crack initiation sites with lower cycles to crack initiation particularly less than 15 000 cycles. This result is arrived at through consideration of the PSB–GB interaction model and is consistent with various supporting experimental results, for example, Heinz and Neumann,[38] Miao *et al.*[13] and Boettner *et al.*,[15] regarding the tendency of Σ3 TBs to nucleate cracks. We emphasize that not all TBs in the simulation exhibit the same life, and we are able to isolate the specific ones in which the energy terms, considered in the model, lead to the relatively shorter life compared with other TBs present in the microstructure.

In this study, fatigue crack initiation is correlated with the size of the critical grain cluster exhibiting the lowest number of cycles to crack initiation. The critical grain cluster size, L_{cs}, is not predefined – it is an outcome of the fatigue model depending on the simulated microstructure and the magnitude of loading. A grain cluster can be either a single grain, or a number of grains connected with LAGBs allowing slip transmission. With crystal orientation measurements, LAGBs can be selected and used within the fatigue model to establish the critical cluster size that results in crack initiation. We show the influence of cluster size as an example with a −0.5 dependence in agreement with other works.[39]

In the concept of grain clusters, GBs that allow slip transmission lead to the formation of grain clusters and do not nucleate cracks. This assumption is justified as the blocking GBs (where pile-ups form) are expected to be more damaging. However, it should be pointed out that in some cases, slip transmission will leave a residual dislocation in the GB plane. The magnitude of the residual Burgers vector ($\mathbf{b_r}$) due to slip transmission has a predominant effect on the GB resistance against slip transmission[40] and consequently on the strain magnitudes across the GB.[36] It is also expected that this would have an influence on the propensity to nucleate cracks in the vicinity of the transmitting GBs. In fact, some researchers have utilized some of these concepts in proposing crack initiation parameters.[11,41] In Hastelloy X, we observe some cases of fatigue cracks near transmitting GBs. For example, the SEM micrograph shown in Fig. 11a F11 shows a grain with slip traces clearly penetrating a TB and transmitting into the twin. This reaction can result in a residual Burgers vector (see schematic in Fig. 11b) that might have played a role in the initiation of the micro crack also shown in the image of Fig. 11a. Establishing estimates of the residual Burgers vector due to slip transmission has been demonstrated in

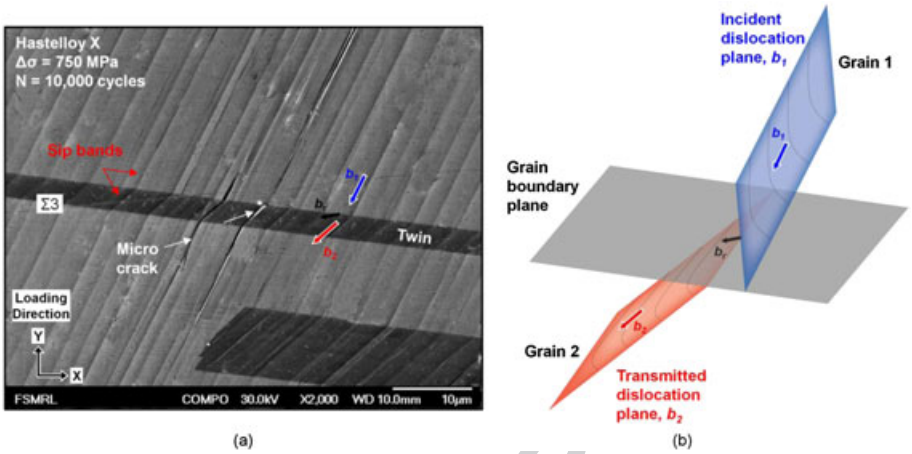

Fig. 11 (a) Scanning electron microscope micrograph showing microcracks in the vicinity of slip bands–grain boundaries interaction regions. Continuous slip traces across the twin boundary indicate possible slip transmission across the interface. (b) Schematic of slip transmission through a grain boundary, where $\mathbf{b_1}$ and $\mathbf{b_2}$ are the Burgers vector of the incident and transmitted dislocations across the grain boundary (GB) plane, and $\mathbf{b_r}$ is the residual dislocation left in the GB plane due to slip transmission.

Ref. [36] using DIC. Further experimental work in fatigue that combines high resolution strain measurements, crystal orientation measurements and analysis of $\mathbf{b_r}$ and the associated strains across the interface, for the GBs that nucleate cracks, can help us better understand some the pertinent issues regarding fatigue crack initiation. Particularly, the importance of the residual Burgers vector can be ascertained. In addition, an improved definition of a grain cluster that considers not only the well-known condition of LAGB but also accounts for the other contributing factors that control the transmission of slip through interfaces should be evaluated.

In the results reported in Fig. 4, we provide an example of high resolution strain measurements in GB regions and demonstrate how these results, when combined with crystal orientation measurements, can be utilized to distinguish between two possible reactions, blockage and slip transmission. The difference between these reactions, as well as between cases of transmission with dissimilar magnitudes of $\mathbf{b_r}$, influences the resulting residual strain field that we measure using DIC.[36] Traditionally, these types of reactions have been studied using higher resolution experimental techniques such as the TEM[40,42,43] and more recently through atomistic simulation.[30,44,45] Although more details can be obtained with the TEM and atomistic simulations, the number of GBs that can be practically investigated is limited. Utilizing DIC and EBSD allows the consideration of a substantial region consisting of 100 grains. Therefore, conclusions that are statistically sound can be drawn. This advantage becomes even more important when the focus is on crack initiation. Experimental measurements over a large region give a better chance to capture the critical GBs that nucleate cracks. Consequently, the correlation between some of important aspects, that is, blocking, transmission, magnitude of $\mathbf{b_r}$, strain levels in the vicinity of GBs and crack initiation in fatigue can be investigated. The techniques and analysis methodologies described in the current paper provide the required foundation for such an effort.

Despite the advantages of DIC and EBSD as employed in this work, the measurements are restricted to the surface of the sample. No direct insight into the thickness direction is possible, as in any two-dimensional, surface measurement technique. The impact of this limitation in fatigue is expected to be minor considering the vast experimental evidence of fatigue cracks initiating at the surface. Also, and related to the DIC measurements, the strains normal to the surface of the specimen (i.e. ε_{zz} in the z direction) were not directly measured, although they can be estimated by assuming plastic incompressibility (see Ref. [36] for example). One can argue that this component is important as it may relate to the formation of extrusion/intrusions on the sample's surface. Atomic force microscopy has been typically used to measure the height profile of such features in fatigue.[46–49] Incorporation of both measurement techniques (surface strains from DIC and atomic force microscopy measurements of extrusions) can be particularly useful. For example, the correlation between the well-know damage initiation sites in fatigue (i.e. extrusions) and surface strain measurements using DIC can provide quantitative insight into the critical conditions (i.e. local strain

magnitudes and extrusion height) resulting in the formation of cracks. These aspects should be the subject of future investigations.

CONCLUSIONS

In this work, a recently developed crack initiation fatigue model and novel high resolution experimental measurements were used to investigate the scatter in fatigue life for the nickel-based superalloy, Hastelloy X. The major contributions and outcomes of this study are summarized as follows:

- The work provided experimental evidence of strain accumulation at GBs in Hastelloy X. High strains across GBs were associated with slip transmission (which leads to the formation of grain clusters), and the formation of pile-ups impinging on GBs was correlated with cases were high strains were observed on one side of the interface only.
- The fatigue model used[6,27,28] can predict the experimentally observed scatter in fatigue life relying only on the microstructural variations established through simulated microstructures (on the basis of EBSD measurements but with grains rearranged spatially).
- The variation in fatigue life was linked to a grain cluster size, L_{cs}, defined as a series of grains bounded by GBs unfavourable for slip transmission. Experimental observation from DIC showed evidence of strain localization in grain clusters that supports the modelling approach. The critical grain cluster size L_{cs} is an *outcome* of the model used and provides a possible means for the statistical 'upscaling' of the microstructurally based life predictions to a macroscale model.
- Evolution of the local plastic strains in the vicinity of GBs under fatigue loading was demonstrated using the full field measurement techniques at the grain level. Local ratcheting at the crystal level was observed with relatively constant nominal average strain.

Acknowledgements

This work was supported by the Midwest Structural Sciences Center (MSSC), which is supported by the Air Vehicles Directorate of the US Air Force Research Laboratory under contract number FA8650-06-2-3620.

REFERENCES

1 Mughrabi, H., Wang, R., Differt, K. and Essmann, U. (1983) Fatigue crack initiation by cyclic slip irreversibilities in high-cycle fatigue. *ASTM*, 5. Q10

2 Laird, C., Finney, J. M. and Kuhlmann-Wilsdorf, D. (1981) Dislocation behavior in fatigue VI: Variation in the localization of strain in persistent slip bands. *Mater. Sci. Eng.* **50**, 127. Q11

3 Cheng, A. S. and Laird, C. (1981) Fatigue life behavior of copper single crystals. Part II: model for crack nucleation in persistent slip bands. *Fatigue Fract. Eng. M.* **4**, 343.

4 Finney, J. M. and Laird, C. (1975) Strain localization in cyclic deformation of copper single crystals. *Philos. Mag.* **31**, 339.

5 Kwai, S. C. (2009) Roles of microstructure in fatigue crack initiation. *Int. J. Fatigue* **32**, 1428.

6 Sangid, M. D., Maier, H. J. and Sehitoglu, H. (2011) An energy-based microstructure model to account for fatigue scatter in polycrystals. *J. Mech. Phys. Solids* **59**, 595.

7 McDowell, D. L. and Dunne, F. P. E. (2010) Microstructure-sensitive computational modeling of fatigue crack formation. *Int. J. Fatigue* **32**, 1521.

8 Christ, H. J., Duber, O., Fritzen, C. P., et al. (2009) Propagation behaviour of microstructural short fatigue cracks in the high-cycle fatigue regime. *Comp. Mater. Sci.* **46**, 561. Q12

9 Dunne, F. P. E., Wilkinson, A. J. and Allen, R. (2007) Experimental and computational studies of low cycle fatigue crack nucleation in a polycrystal. *Int. J. Plasticity* **23**, 273.

10 Findley, K. and Saxena, A. (2006) Low cycle fatigue in rene 88DT at 650 °C: Crack nucleation mechanisms and modeling. *Metall. Mater. Trans. A* **37**, 1469.

11 Bieler, T. R., Eisenlohr, P., Roters, F., et al. (2009) The role of heterogeneous deformation on damage nucleation at grain boundaries in single phase metals. *Int. J. Plasticity* **25**, 1655. Q13

12 Suresh, S. (1998) Fatigue of Materials. Second edn. Cambridge University Press. Q14

13 Miao, J., Pollock, T. M. and Wayne Jones, J. (2009) Crystallographic fatigue crack initiation in nickel-based superalloy Rene 88DT at elevated temperature. *Acta Mater.* **57**, 5964.

14 Llanes, L. and Laird, C. (1992) The role of annealing twin boundaries in the cyclic deformation of f.c.c. materials. *Mater. Sci. Eng. A* **157**, 21.

15 Boettner, R. C., McEvily, A. J. and Liu, Y. C. (1964) On the Formation of Fatigue Cracks at Twin Boundaries. *Philos. Mag.* **10**, 95.

16 Thompson, N., Wadsworth, N. and Louat, N. (1956) Xi. The origin of fatigue fracture in copper. *Philos. Mag.* **1**, 113.

17 Thompson, A. l. (1972) The influence of grain and twin boundaries in fatigue cracking. *Acta Metall.* **20**, 1085.

18 Peralta, P., Llanes, L., Bassani, J. and Laird, C. (1994) Deformation from twin-boundary stresses and the role of texture: Application to fatigue. *Philos. Mag. A* **70**, 219.

19 Guilhem, Y., Basseville, S., Curtit, F., Stephan, J. M. and Cailletaud, G. (2010) Investigation of the effect of grain clusters on fatigue crack initiation in polycrystals. *Int. J. Fatigue* **32**, 1748.

20 Wang, L., Daniewicz, S. R., Horstemeyer, M. F., Sintay, S. and Rollett, A. D. (2009) Three-dimensional finite element analysis using crystal plasticity for a parameter study of microstructurally small fatigue crack growth in a AA7075 aluminum alloy. *Int. J. Fatigue* **31**, 651.

21 Bridier, F., McDowell, D. L., Villechaise, P. and Mendez, J. (2009) Crystal plasticity modeling of slip activity in Ti-6Al-4V under high cycle fatigue loading. *Int. J. Plasticity* **25**, 1066.

22 Cheong, K.-S., Smillie, M. J. and Knowles, D. M. (2007) Predicting fatigue crack initiation through image-based micromechanical modeling. *Acta Mater.* **55**, 1757.

23 Manonukul, A. and Dunne, F. P. E. (2004) High- and Low-Cycle Fatigue Crack Initiation Using Polycrystal Plasticity. *Proceedings: Mathematical, Physical and Engineering Sciences* **460**, 1881.

24 Lin, T. H. and Ito, Y. M. (1969) Mechanics of a fatigue crack nucleation mechanism. *J. Mech. Phys. Solids* **17**, 511.

25 Tanaka, K. and Mura, T. (1981) Dislocation model for fatigue crack initiation. *J. Appl. Mech. T. ASME* **48**, 97.

26 Mughrabi, H., Wang, R., Differt, K. and Essmann, U. (1983) Fatigue crack initiation by cyclic slip irreversibilities in high-cycle fatigue. *ASTM Special Technical Publication*, 5.

27 Sangid, M. D., Maier, H. J. and Sehitoglu, H. (2011) A physically based fatigue model for prediction of crack initiation from persistent slip bands in polycrystals. *Acta Mater.* **59**, 328.

28 Sangid, M. D., Maier, H. J. and Sehitoglu, H. (2011) The role of grain boundaries on fatigue crack initiation - An energy approach. *Int. J. Plasticity* **27**, 801.

29 Brandon, D. G. (1966) The structure of high-angle grain boundaries. *Acta Metall.* **14**, 1479.

30 Sangid, M. D., Ezaz, T., Sehitoglu, H. and Robertson, I. M. (2011) Energy of slip transmission and nucleation at grain boundaries. *Acta Mater.* **59**, 283.

31 Davidson, D., Tryon, R., Oja, M., Matthews, R. and Ravi Chandran, K. (2007) Fatigue Crack Initiation In WASPALOY at 20 °C. *Metall. Mater. Trans. A* **38**, 2214.

32 Zhang, Z. F. and Wang, Z. G. (2008) Grain boundary effects on cyclic deformation and fatigue damage. *Prog. Mater. Sci.* **53**, 1025.

33 Carroll, J., Abuzaid, W., Lambros, J. and Sehitoglu, H. (2010) An experimental methodology to relate local strain to microstructural texture. *Rev. Sci. Instrum.* **81**. Q15

34 Efstathiou, C., Sehitoglu, H. and Lambros, J. (2010) Multiscale strain measurements of plastically deforming polycrystalline titanium: Role of deformation heterogeneities. *Int. J. Plasticity* **26**, 93.

35 Engler, O. and Randle, V. (2010) Introduction to Texture Analysis. Second edn. CRC Press. Q16

36 Abuzaid, W., Sangid, M. D., Carroll, J. D., Sehitoglu, H. and Lambros, J. (2012) Slip transfer and plastic strain accumulation across grain boundaries in hastelloy X. *J. Mech. Phys. Solids* **60**, 1201–1220.

37 Sutton, M. A., Orteu, J.-J., Schreier, H. (2009) Image Correlation for Shape, Motion and Deformation Measurements: Basic Concepts, Theory and Applications. Q17

38 Heinz, A. and Neumann, P. (1990) Crack initiation during high cycle fatigue of an austenitic steel. *Acta Metall. Mater.* **38**, 1933.

39 Armstrong, R (1970) The influence of polycrystal grain size on several mechanical properties of materials. *Metall. Mater. Trans. B* **1**, 1169.

40 Lee, T. C., Robertson, I. M. and Birnbaum, H. K. (1989) Prediction of slip transfer mechanisms across grain boundaries. *Scripta Metall. Mater.* **23**, 799.

41 Boehlert, C. J., Longanbach, S. C. and Bieler, T. R. (2008) Effect of thermomechanical processing on the creep behaviour of Udimet alloy 188. *Philos. Mag.* **88**, 641.

42 Lee, T. C., Robertson, I. M. and Birnbaum, H. K. (1990) An In Situ transmission electron microscope deformation study of the slip transfer mechanisms in metals. *Metall. Trans. A* **21**, 2437.

43 Shen, Z, Wagoner, R. H. and Clark, W. A. T. (1986) Dislocation pile-up and grain boundary interactions in 304 stainless steel. *Scripta Metall. Mater.* **20**, 921.

44 Curtin, W. A. and Dewald, M. (2011) Multiscale modeling of dislocation/grain-boundary interactions: III. 60° dislocations impinging on Σ3, Σ9 and Σ11 tilt boundaries in Al. *Model. Simul. Mater. Sc.* **19**, 055002.

45 Jin, Z. H., Gumbsch, P., Albe, K., et al. (2008) Interactions between non-screw lattice dislocations and coherent twin boundaries in face-centered cubic metals. *Acta Mater.* **56**, 1126. Q18

46 Cretegny, L. and Saxena, A. (2001) AFM characterization of the evolution of surface deformation during fatigue in polycrystalline copper. *Acta Mater.* **49**, 3755.

47 Polak, J. (2003) 4.01 - Cyclic Deformation, Crack Initiation, and Low-cycle Fatigue. In: Comprehensive Structural Integrity (Edited by I. Milne, R. O. Ritchie, B. Karihaloo). Pergamon: Oxford, 1.

48 Polak, J., Man, J. and Obrtlik, K. (2003) AFM evidence of surface relief formation and models of fatigue crack nucleation. *Int. J. Fatigue* **25**, 1027.

49 Risbet, M., Feaugas, X., Guillemer-Neel, C. and Clavel, M. (2003) Use of atomic force microscopy to quantify slip irreversibility in a nickel-base superalloy. *Scr. Mater.* **49**, 533.

50 Ezaz, T., Sangid, M. D. and Sehitoglu, H. (2010) Energy barriers associated with slip-twin interactions. *Philos. Mag.* **91**, 1464–1488.

51 Huang, E. W., Barabash, R. I., Wang, Y., et al. (2008) Plastic behavior of a nickel-based alloy under monotonic-tension and low-cycle-fatigue loading. *Int. J. Plasticity* **24**, 1440. Q19

APPENDIX

As stated earlier, the initiation model is based on the stability of the persistent slip band. The energy terms include contributions from mesoscale factors as well as atomistic interactions. In Table 1, the terms are classified into these two main categories. The continuum terms incorporate the Schmid factors because the orientation of each grain (hence the 12 slip systems) are all defined based on EBSD. The basis for the molecular dynamics calculations for transmission, nucleation at the grain boundaries and energy barriers for glide has been described in Ref. [50]. We demonstrate (via schematics) only the cases for interaction with Σ3 boundaries in Table 1. T1

The fatigue model used in this study was originally developed for another nickel-based superalloy that is Udimet 720.[6,27,28] To use this model for a different material particularly for Hastelloy X in this study, related experimental data are required (tabulated in Table 2). These experimental data are evolution of stress range ($\Delta\sigma$), PSB width (h), dislocation density (ρ) and number of dislocations penetrating the GB (n_{dis}^{pen}) with number of cycles. The $\Delta\sigma$ plays a role in the energy of the stress field due to the applied forces (E_{app}) and has different evolution for different applied strain ranges. One of them for 1% is shown in Fig. 7b. Stress range exhibits hardening up 100 cycles than softens with a very small slope compared with the hardening before crack initiation. A curve is fitted to the experimental data for the hardening range, and then it is assumed that it is constant at the highest value for the remaining cycles. Evolution of h is used to determine the evolution of number of dislocation layers in the PSB. Each dislocation layer has a contribution to the continuum energy terms. Evolution of dislocation density, ρ and evolution of extrusion height Y are obtained via curve fitting from the studies of Huang *et al.*[51] and Risbet *et al.*,[49] respectively.

Table 1 Model details

Model details	Purpose	
Continuum terms in Eq. (1)	Account for the internal stress field ($\bar{\tau}$) that dislocations must overcome to deform the material by increment ∂X	$E_\tau = \bar{\tau}\,\vec{b}\,Ln^{\text{layers}}\partial X$ $\bar{\tau} = \tau^{\text{dis}} - \tau^{b} - \tau^{A}$ $n^{\text{layers}} = h/\vec{b}$
	• The stress field created by dislocation dipoles within the PSB (τ^{dis})	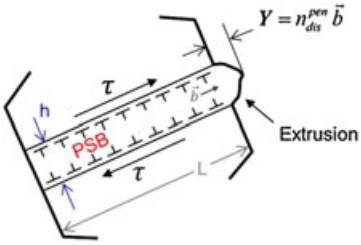
	• Hardening within the PSB due to dislocation interaction (τ^{b}) • The applied shear stress (τ^{A})	
Atomistic terms in Eq. (1)	Dislocation nucleation from GB • GB act as a source for dislocations • Dislocations agglomerate in the PSB • Different GBs types have different energy barriers for dislocation nucleation	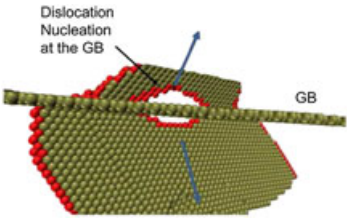
	Dislocation–GB interaction to form extrusions • Dislocations glide and interact with GB • Dislocations penetrating the GB results in the formation of extrusions • Different GBs types have different energy barriers for dislocation to penetrate the GB	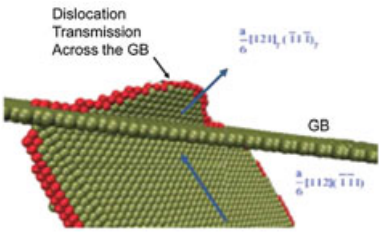
	Dislocations shearing the lattice • Accounts for the energy barrier for dislocations to shear the lattice (dislocation glide) and form PSBs	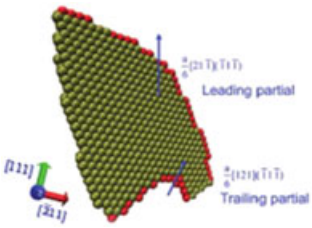

Table 2 Constants for the fatigue model

Variable	Equation	Constants for $0.008 \le \Delta\varepsilon \le 0.012$	Where in the model
Stress range, $\Delta\sigma$ (MPa) 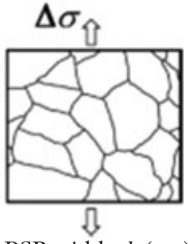	$\Delta\sigma = a_1\Delta\varepsilon + a_2 N^{-0.1} + a_3$ when $N < 100$ $\Delta\sigma = a_1\Delta\varepsilon + a_2 100^{-0.1} + a_3$ when $N \ge 100$	$a_1 = 28750$ $a_2 = -350$ $a_3 = 862.5$	$E_{app} = (m\Delta\sigma)\vec{b}\ Ln^{\text{layers}}\partial X_i$ (externally applied energy)
PSB width, h (nm) 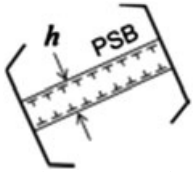	$h = b_1\sqrt{N}$ when $N < 2000$ $h = b_1\sqrt{2000}$ when $N \ge 2000$	$b_1 2 \times 10^{-9}$	$n^{\text{layers}} = \frac{h}{1.56\times10^{-9}}$ (number of dislocation layers in PSB)
Dislocation density, ρ (cm^{-2})	$\rho \propto (c_1 N^{c_2} + c_3)$ Huang *et al.*[51]	$c_1 = -2.321 \times 10^8$ $c_2 = -0.4035$ $c_3 = -2.379 \times 10^8$	$E_{hard} = \left(\alpha\mu\vec{b}\ \sqrt{\rho} + \frac{\sigma_y}{M}\right)\vec{b}\ Ln^{\text{layers}}\partial X_i$ (work hardening energy) $E_{nucleation} = \sum_i \partial X_i E_{MD}^{\text{nucleation}}(\rho - \rho_0)\overset{t}{\vec{b}}\ hL^2$ (dislocation nucleation energy)
Number of dislocations penetrating the GB, n_{dis}^{pen} 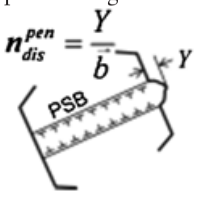	$n_{dis}^{\text{pen}} = 0$ when $N < f_1 e^{f_2\Delta\varepsilon} + f_3$ $n_{dis}^{\text{pen}} \propto (d_1\Delta\varepsilon + d_2)\sqrt{N - f_1 e^{f_2\Delta\varepsilon} - f_3}$ when $N \ge f_1 e^{f_2\Delta\varepsilon} + f_3$ Risbet *et al.*[49]	$d_1 = 187.5$ $d_2 = -0.26$ $f_1 = 3.9 \times 10^6$ $f_2 = -804.7$ $f_3 = 1750$	$E_{interaction} = \sum_i \partial X_i E_{MD}^{\text{interaction}} n_{dis}^{\text{pen}}\vec{b}\ h$ (PSB–GB interaction energy)

Author Query Form

Journal: Fatigue & Fracture of Engineering Materials & Structures

Article: ffe_12048

Dear Author,

During the copyediting of your paper, the following queries arose. Please respond to these by annotating your proofs with the necessary changes/additions.

- If you intend to annotate your proof electronically, please refer to the E-annotation guidelines.
- If you intend to annotate your proof by means of hard-copy mark-up, please refer to the proof mark-up symbols guidelines. If manually writing corrections on your proof and returning it by fax, do not write too close to the edge of the paper. Please remember that illegible mark-ups may delay publication.

Whether you opt for hard-copy or electronic annotation of your proofs, we recommend that you provide additional clarification of answers to queries by entering your answers on the query sheet, in addition to the text mark-up.

Query No.	Query	Remark
Q1	AUTHOR: Please submit the Copyright Transfer Agreement (CTA). The download link for the CTA form is: http://www.wiley.com/go/ctaaglobal.	
Q2	AUTHOR: Please submit the Colour Work Agreement (CWA) if your article contains a colour figure for publication. The download link for the CWA form is:www.blackwellpublishing.com/pdf/SN_Sub2000_X_CoW.pdf	
Q3	AUTHOR: As per journal instruction, the Nomenclature should be in alphabetical order (small letters followed by capital letters and then Greek terms). Please check.	
Q4	AUTHOR: A running head short title was not supplied; please check if this one is suitable and, if not, please supply a short title that can be used instead.	
Q5	AUTHOR: ‘Section 2.4’ has been changed to ‘Fatigue Model Section’ since the section headings are unnumbered. Please check if appropriate.	
Q6	AUTHOR: ‘Section 3.1’ has been changed to ‘Microstructural analysis of fatigued samples section’ since the section headings are unnumbered. Please check if appropriate.	
Q7	AUTHOR: ‘Section 2.2’ has been changed to ‘High Resolution Digital Image Correlation Measurements section’ since the section headings are unnumbered. Please check if appropriate.	
Q8	AUTHOR: ‘Section 3.2’ has been changed to ‘High Resolution Strain Measurements section’ since the section headings are unnumbered. Please check if appropriate.	
Q9	AUTHOR: ‘Section 3.4’ has been changed to ‘Scatter in Fatigue Life section’ since the section headings are unnumbered. Please check if appropriate.	
Q10	AUTHOR: If reference 1 has now been published online, please add relevant year/DOI information. If this reference has now been published in print, please add relevant volume information.	

Query No.	Query	Remark
Q11	AUTHOR: For journal references that uses expanded journal title, please provide titles that are abbreviated with dot.	
Q12	AUTHOR: Please provide the complete list of authors for reference 8.	
Q13	AUTHOR: Please provide the complete list of authors for reference 11.	
Q14	AUTHOR: Please provide the city location of publisher for Reference 12.	
Q15	AUTHOR: If reference 33 has now been published online, please add relevant year/DOI information. If this reference has now been published in print, please add relevant page information.	
Q16	AUTHOR: Please provide the city location of publisher for Reference 35.	
Q17	AUTHOR: Please provide the name and city location of publisher for Reference 37.	
Q18	AUTHOR: Please provide the complete list of authors for reference 45.	
Q19	AUTHOR: Please provide the complete list of authors for reference 51.	

WILEY-BLACKWELL

USING e-ANNOTATION TOOLS FOR ELECTRONIC PROOF CORRECTION

Required software to e-Annotate PDFs: Adobe Acrobat Professional or Adobe Reader (version 7.0 or above). (Note that this document uses screenshots from Adobe Reader X)
The latest version of Acrobat Reader can be downloaded for free at: http://get.adobe.com/uk/reader/

Once you have Acrobat Reader open on your computer, click on the Comment tab at the right of the toolbar:

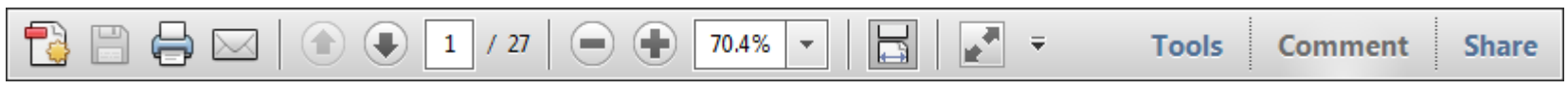

This will open up a panel down the right side of the document. The majority of tools you will use for annotating your proof will be in the Annotations section, pictured opposite. We've picked out some of these tools below:

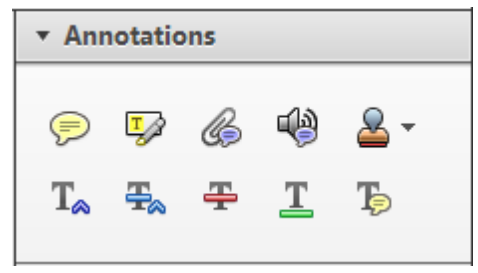

1. Replace (Ins) Tool – for replacing text.

Strikes a line through text and opens up a text box where replacement text can be entered.

How to use it

- Highlight a word or sentence.
- Click on the Replace (Ins) icon in the Annotations section.
- Type the replacement text into the blue box that appears.

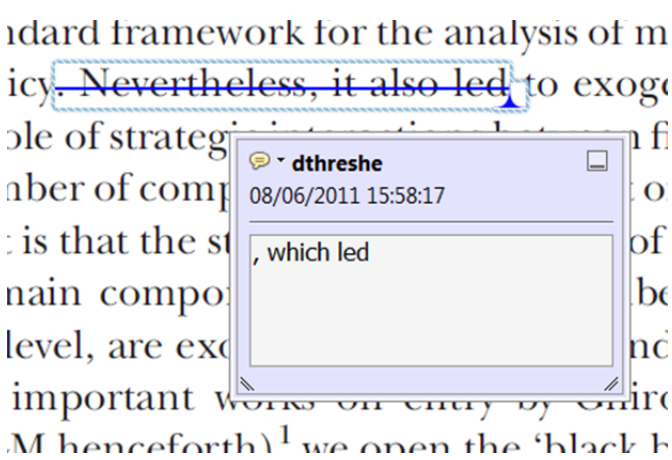

2. Strikethrough (Del) Tool – for deleting text.

Strikes a red line through text that is to be deleted.

How to use it

- Highlight a word or sentence.
- Click on the Strikethrough (Del) icon in the Annotations section.

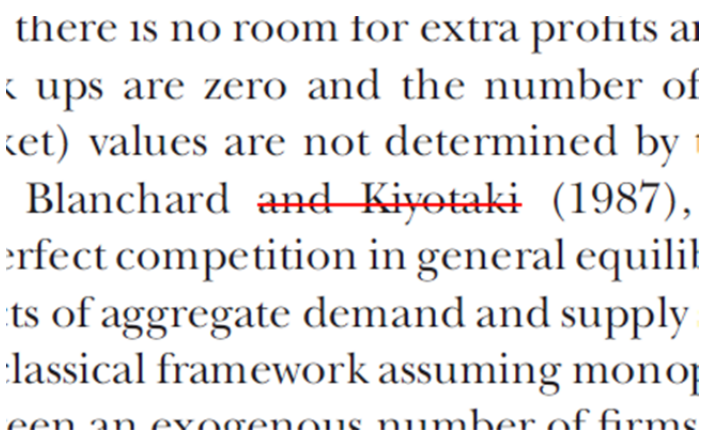

3. Add note to text Tool – for highlighting a section to be changed to bold or italic.

Highlights text in yellow and opens up a text box where comments can be entered.

How to use it

- Highlight the relevant section of text.
- Click on the Add note to text icon in the Annotations section.
- Type instruction on what should be changed regarding the text into the yellow box that appears.

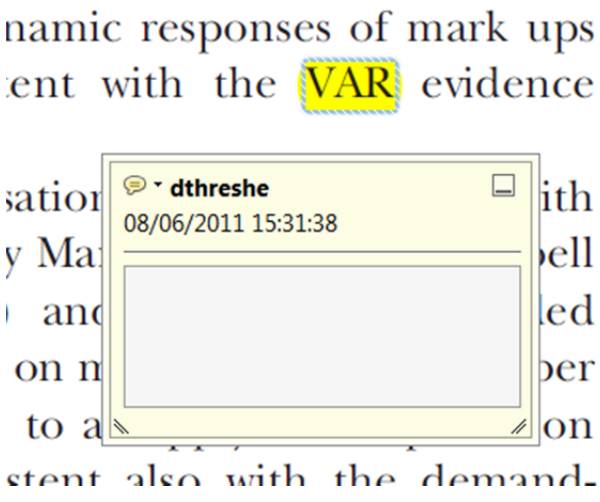

4. Add sticky note Tool – for making notes at specific points in the text.

Marks a point in the proof where a comment needs to be highlighted.

How to use it

- Click on the Add sticky note icon in the Annotations section.
- Click at the point in the proof where the comment should be inserted.
- Type the comment into the yellow box that appears.

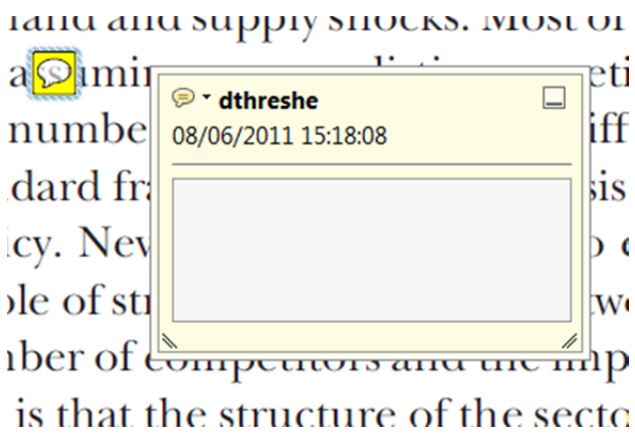

5. Attach File Tool – for inserting large amounts of text or replacement figures.

Inserts an icon linking to the attached file in the appropriate pace in the text.

How to use it

- Click on the Attach File icon in the Annotations section.
- Click on the proof to where you'd like the attached file to be linked.
- Select the file to be attached from your computer or network.
- Select the colour and type of icon that will appear in the proof. Click OK.

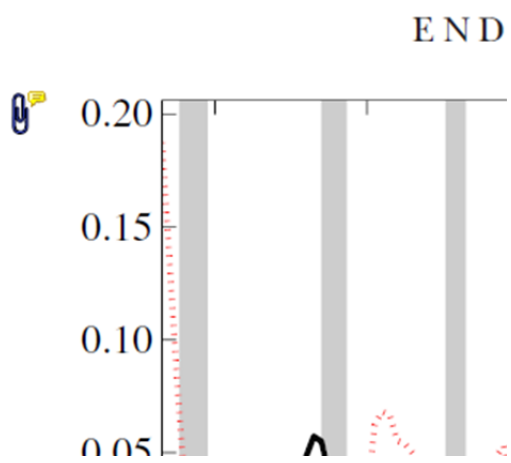

6. Add stamp Tool – for approving a proof if no corrections are required.

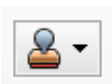

Inserts a selected stamp onto an appropriate place in the proof.

How to use it

- Click on the Add stamp icon in the Annotations section.
- Select the stamp you want to use. (The Approved stamp is usually available directly in the menu that appears).
- Click on the proof where you'd like the stamp to appear. (Where a proof is to be approved as it is, this would normally be on the first page).

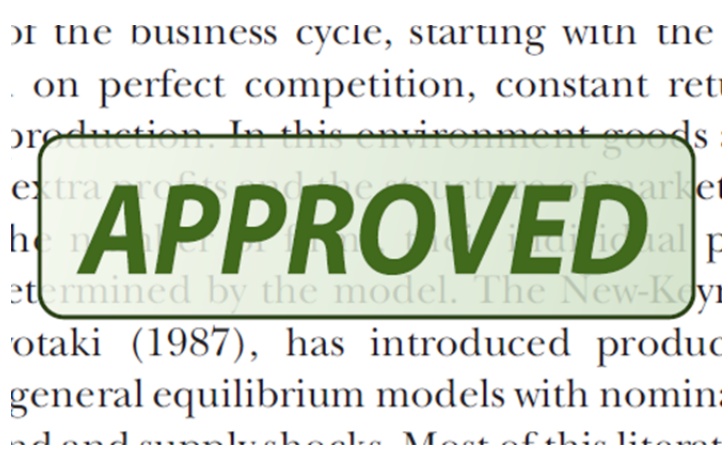

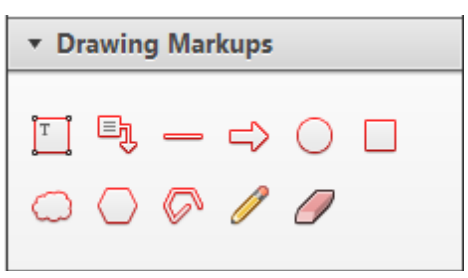

7. Drawing Markups Tools – for drawing shapes, lines and freeform annotations on proofs and commenting on these marks.

Allows shapes, lines and freeform annotations to be drawn on proofs and for comment to be made on these marks..

How to use it

- Click on one of the shapes in the Drawing Markups section.
- Click on the proof at the relevant point and draw the selected shape with the cursor.
- To add a comment to the drawn shape, move the cursor over the shape until an arrowhead appears.
- Double click on the shape and type any text in the red box that appears.

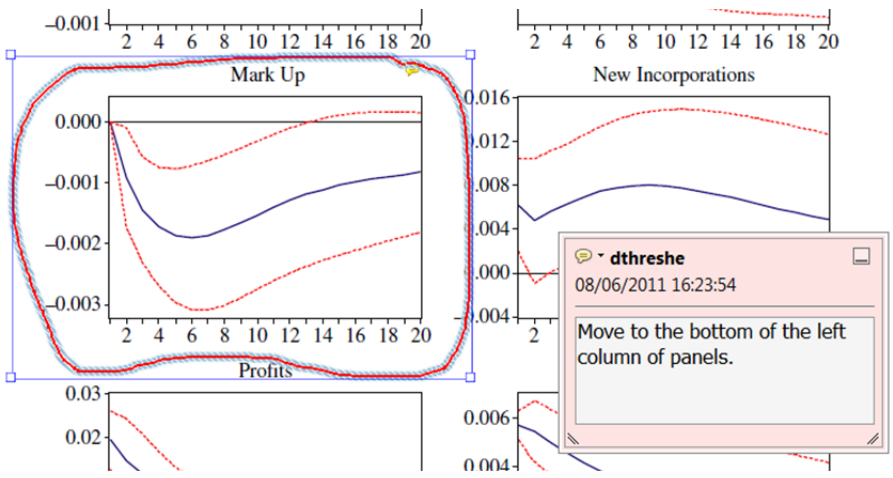

For further information on how to annotate proofs, click on the Help menu to reveal a list of further options: